Available online at www.CivileJournal.org

# Civil Engineering Journal

(E-ISSN: 2476-3055; ISSN: 2676-6957)

Vol. 11, No. 04, April, 2025


# Investigation of an Innovative Technique for R.C. Square Footing Reinforced by GFRP and BFRP Bars with HSC

Mona I. Badawi [1], Marwa I. Badawi [1], Mahmoud Awwad [1*]

[1] *Department of Civil Engineering, Benha Faculty of Engineering, Benha University, Benha, Egypt*.

Received 04 January 2025; Revised 23 March 2025; Accepted 30 March 2025; Published 01 April 2025

**Abstract**

The utilization of alternate reinforcement materials to improve footing capacity performance has garnered significant interest in recent years. Limited research has been conducted to understand the impacts of basalt reinforcement. This study aims to investigate the performance of the high-strength concrete (HSC) footing reinforced by alternative materials such as glass fiber-reinforced polymer (GFRP) bars and basalt fiber-reinforced polymer (BFRP) bars. This work contains experimental and finite element (FE) numerical modeling aimed at investigating the behavior and crack propagation of HSC footings. Axial load investigations were conducted on RC square footings with cross sections of 300×300×90 mm for different materials in reinforcing the RC footing, and an experimental investigation of mechanical properties has been carried out. The main reinforcement for the footing has been varied. Two types of material, namely, glass fiber-reinforced polymer (GFRP) bars and basalt fiber-reinforced polymer (BFRP) bars, were used. Four types of concrete mixture were used: normal concrete (NC), high-strength concrete (HSC), glass fiber-reinforced concrete (GFRC), and HSC+ glass fiber bristles. The experimental results demonstrated an improvement in the ultimate load by 28-49% and an enhancement in performance represented in the cracking pattern. Additionally, a 3D nonlinear finite element (FE) analysis utilizing Abaqus software was conducted to verify the numerical results with experimental findings; the results proved the suitability of the employed experimental setup.

*Keywords:* GFRP Bars; BFRP Bars; FRP Concrete; Square Footing; FEM.

## 1. Introduction

In recent decades, corrosion in severe conditions has substantially impacted reinforced concrete (RC) constructions, leading to lower strength and efficiency. To address these challenges, extensive research has focused on enhancing concrete strength and mitigating corrosion-related issues. High-strength concrete (HSC) has emerged as a highly advantageous material, offering superior performance compared to regular-strength concrete. HSC's enhanced robustness allows designers to reduce the cross-sectional dimensions of structural elements without compromising their strength. On the industrial front, the development of HSC reinforced with non-corroding glass fiber-reinforced polymer (GFRP) bars has further extended the service life of structural components. GFRP bars, as alternative reinforcement, provide exceptional resistance to corrosion and chemical attacks, making them ideal for structures exposed to harsh environments. This innovative combination of HSC and GFRP significantly enhances the durability and efficiency of reinforced concrete systems [1].

In the broader field of modern construction, the pursuit of materials that balance performance, durability, and sustainability has driven the adoption of non-metallic reinforcement alternatives. GFRP and geosynthetic geogrid reinforcement have become known as promising substitutes for conventional steel reinforcement in concrete structures

* Corresponding author: mahmoud.awad@bhit.bu.edu.eg

http://dx.doi.org/10.28991/CEJ-2025-011-04-017

[2, 3]. These materials are particularly advantageous in environments susceptible to corrosion, as they offer superior resistance to chemical attacks, ensuring longer service life for reinforced concrete structures. Additionally, the development of advanced concrete materials has significantly contributed to the enhancement of structural performance in modern construction. Among these innovations, High-Strength Concrete (HSC) and Fiber-Reinforced Concrete (FRC) incorporating glass fibers have gained considerable attention for their ability to improve the durability, strength, and overall efficiency of structural elements, including foundations.

In particular, square concrete footings—critical components for transferring loads from superstructures to the underlying soil—can benefit greatly from these concrete materials due to their enhanced load-bearing capacity and resistance to cracking. Steel reinforcement has traditionally been used to enhance the tensile strength of such foundations. However, issues like corrosion and long-term degradation in aggressive environments have prompted researchers and engineers to explore alternatives like GFRP and geosynthetic geogrids reinforcement due to their high tensile strength-to-weight ratios, good fatigue resistance, and thermal stability [4, 5]. Such reinforcement alternatives have proven successful in strengthening square footings [6, 7].

GFRP bars are manufactured using glass fibers and a polymer resin matrix, offering serviceability and lightweight yet robust reinforcement with impressive resistance to corrosion in saline and acidic conditions [8, 9]. On the other hand, BFRP bars, made from basalt fibers, are lauded for their higher thermal stability, environmental friendliness, and comparable tensile strength [10–12]. The superior qualities of basalt fiber [13, 14], along with cost-effective manufacturing processes, have resulted in the creation of BFRP bars as interior reinforcement for concrete structures. Many researchers have demonstrated the mechanical characterization of basalt FRP rebars [15–17]. Both materials help reduce maintenance costs and extend the lifespan of structures subjected to harsh environmental conditions [18-20]. Also, the characteristics of basalt fiber as a strengthening material for concrete structures have been explored [21, 22].

Studies have demonstrated that square footings reinforced with GFRP and BFRP bars exhibit significant load-bearing capacity while maintaining crack control and structural integrity under various loading conditions [23]. For instance, Halim et al. [24] found that using GFRP bars in concrete footings improved durability and mitigated corrosion-related failures. Similarly, Wei et al. [25] highlighted the resistance to the environment and mechanical properties of basalt and glass fibers.

High-strength concrete (HSC) is characterized by its superior compressive strength, which makes it suitable for applications where high performance and compact dimensions are required. HSC has better mechanical properties, less permeability, and longer durability in harsh environments because it uses finely graded aggregates and optimized mix designs [26]. These properties make HSC an excellent choice for reinforced concrete foundations subjected to heavy loads and challenging environmental conditions. On the other hand, glass fiber-reinforced concrete (GFRC) is a composite material that integrates glass fibers into the concrete matrix to enhance its tensile strength, crack resistance, and ductility [27]. GFRC has proven particularly effective in improving the performance of concrete subjected to tensile stresses, such as the corners of square footings, where stress concentrations are common. Sagar & Sivakumar [28] demonstrated that glass fiber reinforcement can significantly improve the post-crack behavior of concrete, ensuring structural integrity even under extreme loading conditions.

When combined, the use of HSC and GFRP reinforcement in square footings offers synergistic solutions that capitalize on the compressive strength of HSC and the tensile properties of GFRP. These advancements address traditional challenges associated with cracking, spalling, and reduced service life in reinforced concrete foundations, particularly in areas with high seismic activity or corrosive environments. Recent studies have emphasized the benefits of these materials in foundation designs. For example, Afroughsabet et al. [29] highlighted the improved load distribution and reduced cracking in footings made with HSC reinforced with glass fibers. Similarly, Christian & Chye [30] demonstrated the enhancement in durability and resistance to deformation in square footings constructed using fiber-reinforced HSC.

This research explores the potential of GFRP and BFRP reinforcement in enhancing the performance of square concrete footings, focusing on their mechanical properties. The study aims to compare these advanced materials and evaluate their effectiveness as sustainable alternatives to traditional steel reinforcement. Also, this research aims to explore the combined use of high-strength concrete and glass fiber reinforced concrete in square concrete footings, both experimentally and numerically, focusing on their mechanical performance, durability, and crack behavior. By evaluating these materials' contributions, the study seeks to provide insights into their suitability for improving the longevity and structural efficiency of reinforced concrete foundations.

## 2. Research Methodology

Figure 1 depicts a flowchart of the study which is conducted in two phases to: (i) experimentally investigate the enhancement in square reinforced concrete (RC) footing performance using GFRP and BFRP in combination with normal concrete, HSC, GFRC, and HSC+ glass fiber bristles (GFPR); and (ii) numerically represent and verify the experimental results using finite element modelling (FEM).

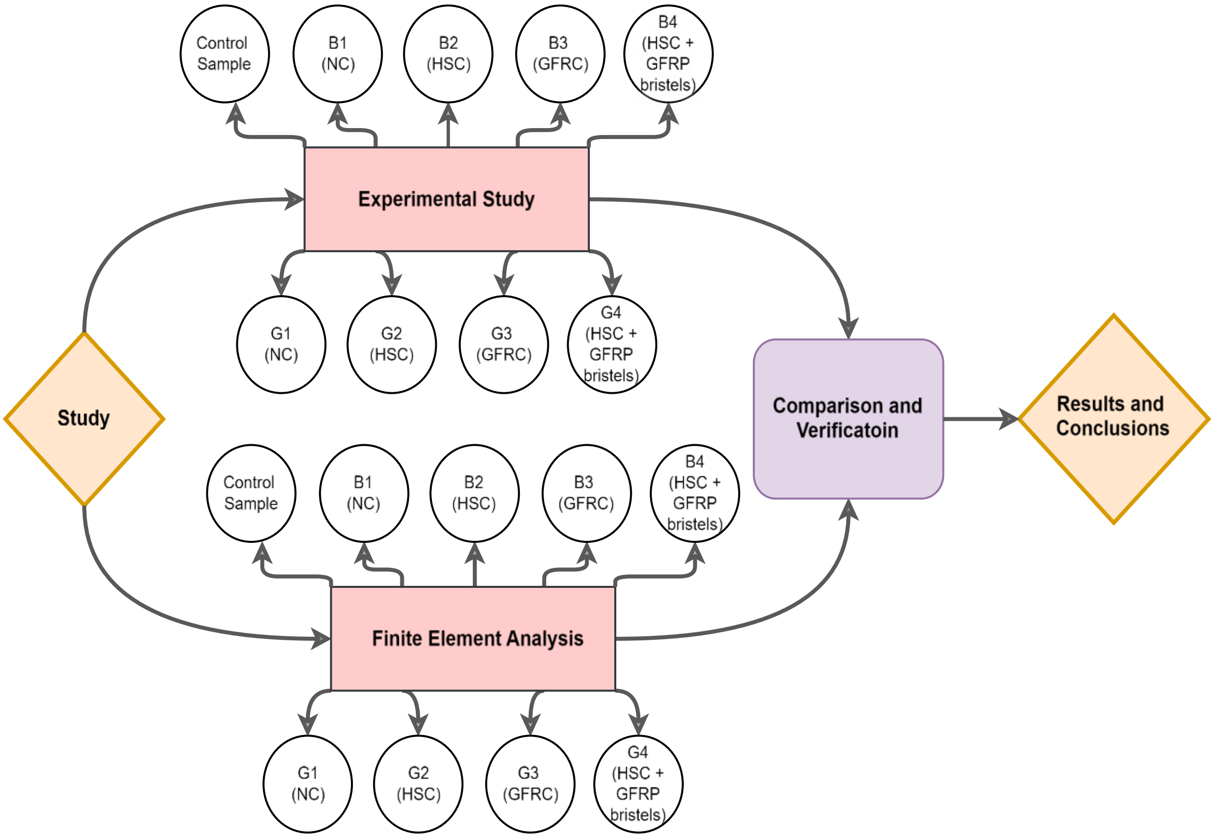


**Figure 1. Flowchart detailing the extent of the work in the study**

## 2.1. Specimen Configurations and Test Matrix

To reach the aim of this study, a total of nine square footings, having dimensions of 300x300x90 mm, were exposed to compressive stresses up to failure (Figure 2). The nine footings represented various combinations of square footings reinforced with steel, GFRP, and BFRP bars embedded in GFRC or HSC, as detailed in Table 1. The program of experimentation was segmented into two groups of four each and a control square RC footing. The RC footings in the first group were reinforced using BFRP bars. Each footing in this group was reinforced with two BFRP bars, while the concrete type was changed to normal concrete (NC) for sample B1, HSC for sample B2, GFRC for sample B3, and a mix of glass fiber bristles and HSC for sample B4. A similar approach was adopted for the second group; however, GFRP bars were used to reinforce the footing. Similar to the first group, the concrete type was changed for each footing, with normal concrete (NC) for sample G1, HSC for sample G2, GFRC for sample G3, and a mix of glass fiber bristles and HSC for sample G4. This extensive testing scheme allows the performance of each concrete type to be assessed in the presence of the different reinforcement alternatives, while also allowing for the comparison of the various testing combinations to be compared against the control specimen (C). The control specimen was constructed using normal concrete reinforced with 2 steel bars. Worth mentioning is that all bars used had a diameter of 6 mm to eliminate the impact of percentage of reinforcement.

**Table 1. Experimental program indicating the two groups and control sample**

| Group No. | Footing code | Reinforced material | Number of units | Glass fiber bristles (%) | Concrete type |
|---|---|---|---|---|---|
| Control | C | Steel bars | 2T6 mm | | Normal - concrete (NC) |
| First | B1 | Basalt fiber bars | 2T6 mm | - | Normal - concrete (NC) |
| | B2 | | | - | High strength concrete (HSC) |
| | B3 | | | 1.25 | Glass fiber reinforced concrete (GFRC) |
| | B4 | | | 1.25 | High strength concrete + glass fiber bristles |
| Second | G1 | Glass fiber bars | 2T6 mm | - | Normal - concrete (NC) |
| | G2 | | | - | High strength concrete (HSC) |
| | G3 | | | 1.25 | Glass fiber reinforced concrete (GFRC) |
| | G4 | | | 1.25 | High strength concrete + glass fiber bristles |

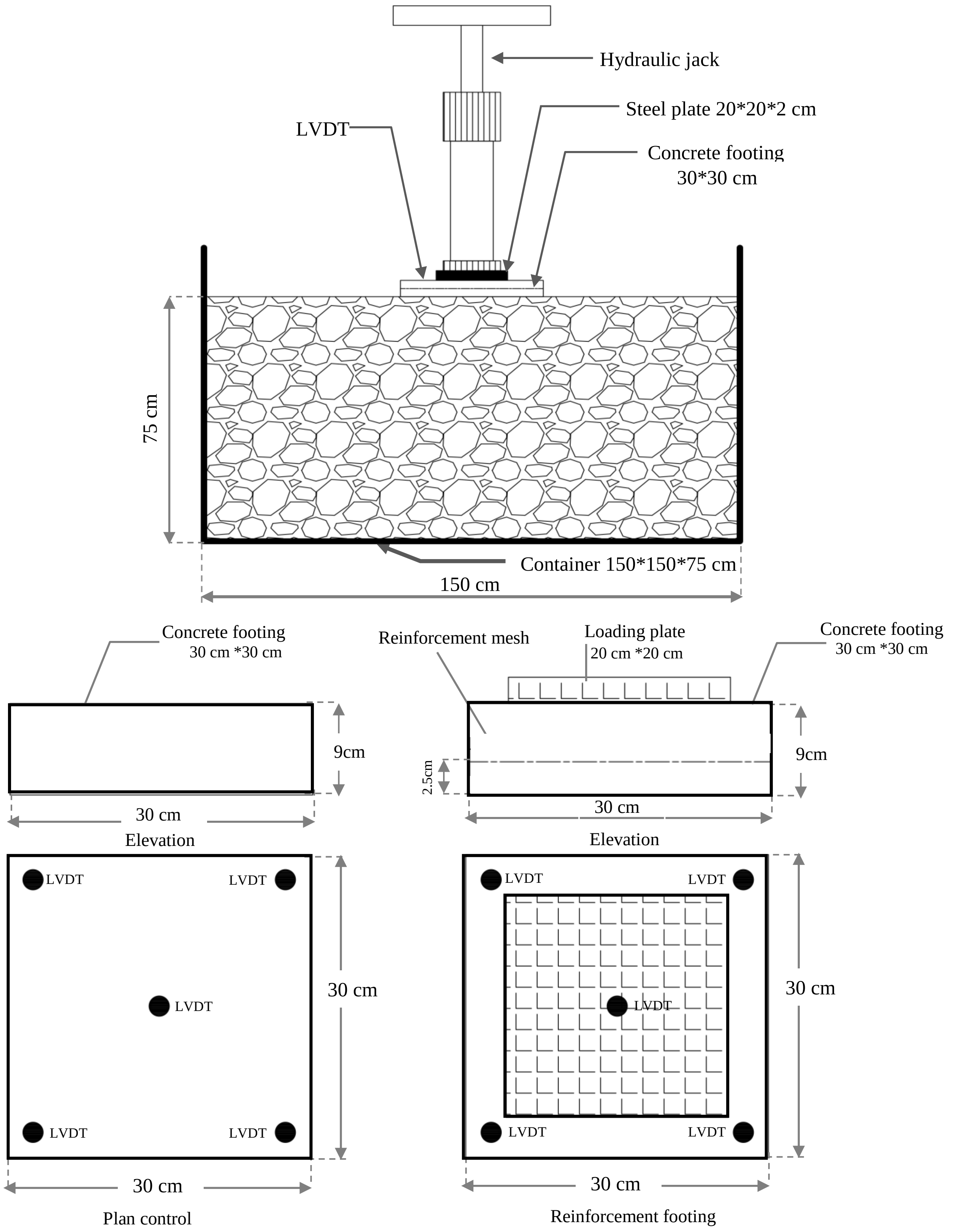


**Figure 2. Schematic of the sample and the test setup**

## 2.2. Material Properties

To replicate in-situ conditions, the footing was tested on a soil mixture housed within a stiff steel tank. The soil mixture comprised coarse aggregates and natural siliceous sand at a ratio of two-to-one to establish a robust foundational layer. The constituents making up the soil mixture were clean and almost free from impurities. The coarse aggregates were a mixture of size 1 with a maximum dimension of 3/4" (19 mm) and size zero with a maximum dimension of 3/8" (10 mm). The general shape of the coarse aggregate mix was round and sub-angular, and the surface texture was nearly smooth. On the other hand, the sand used had a fineness modulus of 2.75. Table 2 gives the properties of the soil mixture used.

**Table 2. Properties of the soil mixture**

| Cohesion | Friction angle | Mean modulus of elasticity (MPa) | Secant young modulus of elasticity (MPa) | Poisson's ratio | Dry density ($N/mm^3$) | Optimum moisture content (%) |
|---|---|---|---|---|---|---|
| 0 | $35^0$ | 3.35 | 3.55 | 0.25 | 2090.820 | 6.90 |

Table 3 presents the proportions of the concrete mix used to cast the specimens. Normal concrete, high-strength concrete, glass fiber reinforced concrete, and high-strength concrete with glass fiber bristles were tested for 28 days compressive strength and exhibited strengths of 30, 35, 39, and 41 MPa, respectively. Three samples were cast and cured during the specimen casting process to evaluate an average of compressive test outcomes after 28 days.

**Table 3. Concrete mix proportions**

| Concrete type | Mix proportions ($kg/m^3$) | | | | | | |
|---|---|---|---|---|---|---|---|
| | Cement | Water | Aggregate | | Additions | | GFRP bristles (%) |
| | | | Coarse | Fine (Sand) | Silica fume | Superplasticizer | |
| Normal concrete | 475 | 155 | 1083 | 690 | - | - | - |
| High strength concrete | 475 | 155 | 1083 | 690 | 48 | 15.675 | - |
| Glass fiber reinforced concrete | 475 | 155 | 1083 | 690 | - | - | 1.25 |
| High strength concrete + Glass fiber bristles | 475 | 155 | 1083 | 690 | 48 | 15.675 | 1.25 |

The reinforcement bars, irrespective of their material, were 6 mm in diameter. The longitudinal and transverse reinforcement in the control sample were plain high-tensile rounded steel bars (R6) and were sourced from a local supplier [31] (Figure 3-a). The GFRP bars (Figure 3-b) and BFRP bars (Figure 3-c) were sourced from international distributors Armastek [32] and ABFC [33], respectively. The GFRP bristles used to mix were 12-16 mm in length and 0.01 mm in thickness (Figure 3-d). Table 4 details the mechanical characteristics of the various reinforcement bars. The stress-strain curves for GFRP and BFRP bars have been demonstrated in Figure 4.

(a) Steel bars (b) GFPR bars (c) Basalt bars (d) (GFPR) glass fiber bristles

**Figure 3. Typical views of the reinforcement (a)steel bars, (b) GFRP bars, (c) BFRP bars, and (d) GFPR glass fiber bristles**

**Table 4. Physical and mechanical properties of the reinforcement material [31–33]**

| Type | Diameter (mm) | Tensile strength (MPa) | Modulus of elasticity (MPa) | Strain at failure (%) |
|---|---|---|---|---|
| Steel bars | | 520* | 20000* | 1.2* |
| GFRP bars | 6* | 1100* | 28570* | 2.9* |
| BFRP bars | | 1400* | 66600* | 2* |

* Data provided in the manufacture data sheet.

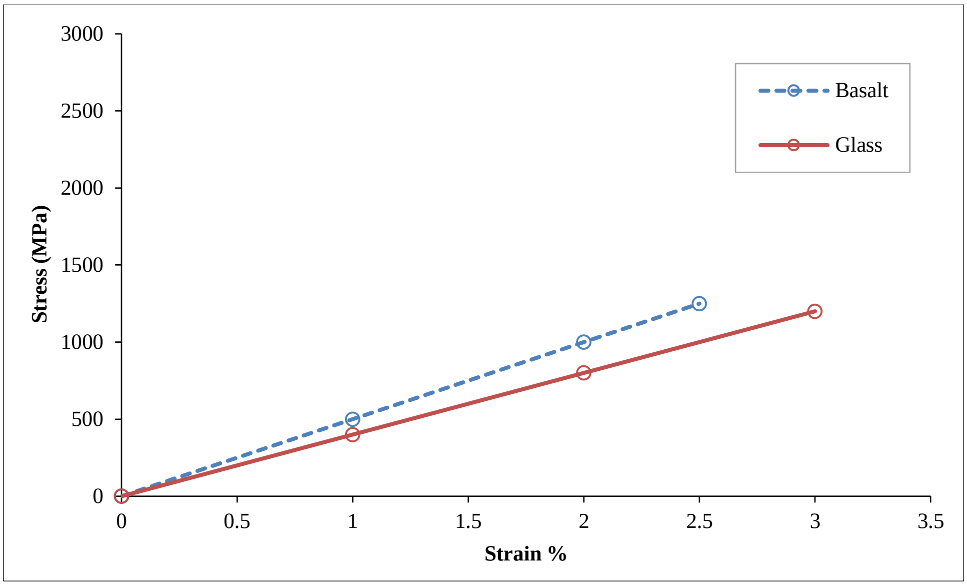


**Figure 4. Stress-Strain curves for GFRP, and BFRP bars**

## 2.3. Test Configuration and Instrumentations

To simulate the behavior of a simply loaded footing, the specimens were placed on a soil mixture within a stiff steel tank (Figure 5). The soil was placed in three 25 cm layers each, with each layer compacted to achieve over 95% compaction. The tank was large enough to accommodate the footing without having any adverse effects caused by end constraints. Constructed from durable steel, the tank measured 1.50 by 1.50 by 0.75 m, in length, width, and height, respectively. The preparation of both the tank and soil followed strict protocols to ensure accuracy and reliability. The stiff steel tank was supported on all four sides by steel I-beams. The specimens were positioned within a stiff reacting frame having a maximum capacity of 1000 kN. The load was applied centrically using a hydraulic jack with the same capacity and connected to an electrical pump. A large steel plate was used to distribute the load from the hydraulic jack onto the square footing head. To measure the applied load, a load cell having a maximum capacity of 1000 kN was positioned beneath the hydraulic jack. A pump displacement control system applied the load at a constant strain rate of 0.035/minute. To measure deflection, five linear variable differential transducers (LVDTs) were positioned above the quarter-span and approximately in the middle of the specimens. The applied load was gradually increased until failure, with crack growth observed and marked for further analysis. All test data were recorded on a desktop computer at two-second intervals using a data acquisition system.

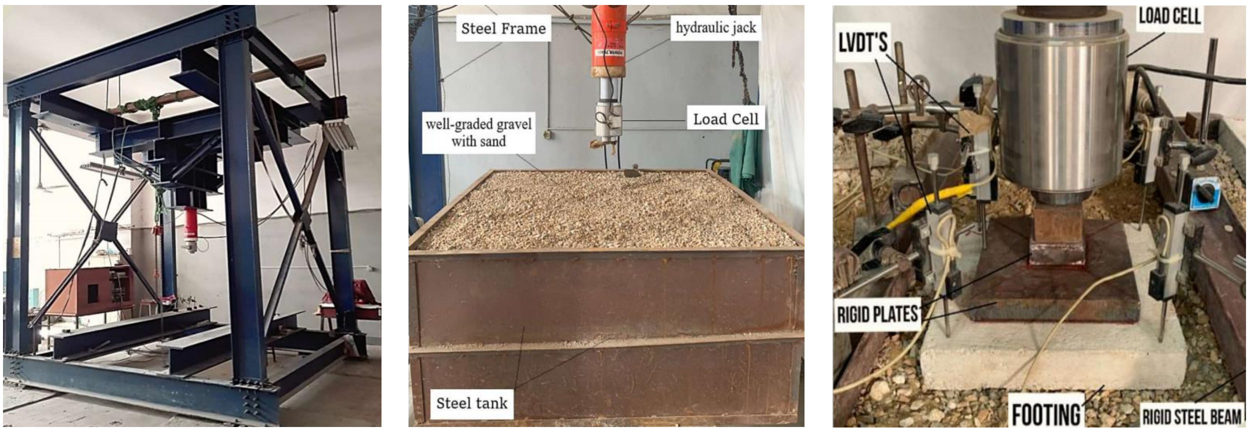


**Figure 5. The test setup used in the axial capacity determination showing the various components**

# 3. Experimental Results and Discussion

The load-deflection curves for concrete footings are shown in Figure 6. These curves include the two types of reinforcing materials (GFRP bars and BFRP bars) and four types of concrete mixtures (normal concrete, high-strength concrete, glass fiber reinforced concrete, and high-strength concrete with glass fiber bristles). Figure 5 delineates the load (P), vertical displacement during the first cracking phase (Δcr), and vertical displacement at the ultimate phase (Δu) for all tested footings. Uncracked stiffness (Ki) and ultimate stiffness (Ku) were determined for all footings. The results for all the experiments are shown in Table 5.

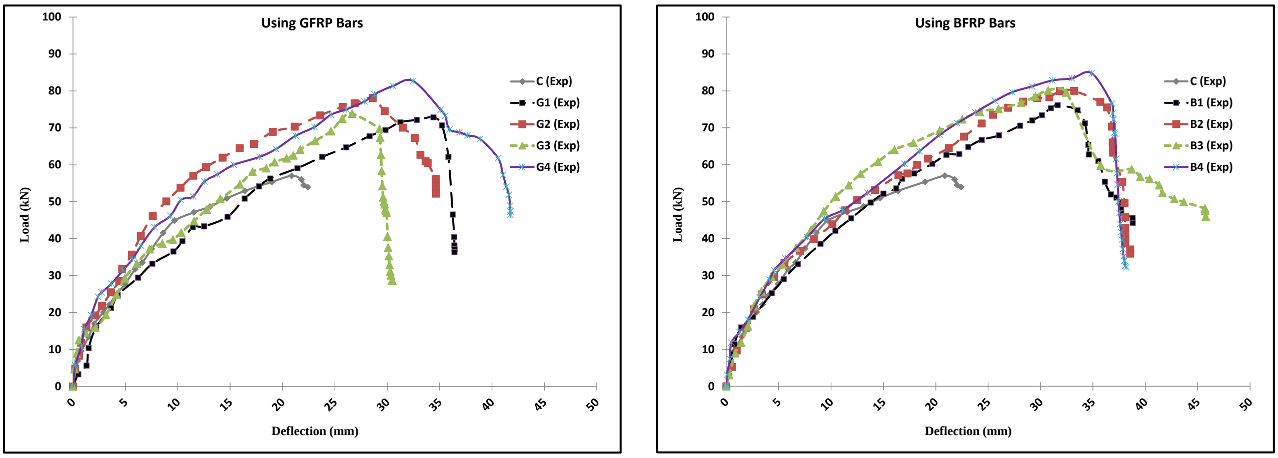


(a) (b)

**Figure 6. Load-deflection curves for the square footings reinforced with; a) GFRP bars, and b) BFRP bars**

**Table 5. Summary of Experimental Results**

| Group No. | Footing Code | First crack | | Ultimate | | $\frac{P_u}{P_{control}}$ | $\Delta_{uc}=\frac{\Delta_u * P_{control}}{P_u}$ | Ultimate stiffness (Ku) | Un-cracked stiffness (Ki) |
|---|---|---|---|---|---|---|---|---|---|
| | | Load (Pcr) (kN) | Deflection (Δcr) (mm) | Load (Pu) (kN) | Deflection (Δu) (mm) | | | $\frac{P_{cr}}{\Delta_{cr}}$ | $\frac{P_u - P_{cr}}{\Delta_u - \Delta_{cr}}$ |
| Control | C | 16.99 | 2.04 | 57.02 | 20.87 | 1.00 | 20.87 | 8.33 | 2.13 |
| First | B1 | 18.78 | 2.56 | 76.15 | 31.63 | 1.34 | 23.68 | 7.34 | 1.97 |
| | B2 | 24.88 | 3.41 | 80.02 | 33.20 | 1.40 | 23.66 | 7.30 | 1.85 |
| | B3 | 21.71 | 2.65 | 80.14 | 30.73 | 1.41 | 21.86 | 8.19 | 2.08 |
| | B4 | 28.85 | 4.14 | 84.79 | 34.87 | 1.49 | 23.45 | 6.97 | 1.82 |
| Second | G1 | 16.04 | 2.21 | 72.85 | 34.41 | 1.28 | 26.93 | 7.26 | 1.76 |
| | G2 | 25.51 | 3.62 | 78.13 | 28.61 | 1.37 | 20.88 | 7.05 | 2.11 |
| | G3 | 19.37 | 3.15 | 73.87 | 26.64 | 1.30 | 20.56 | 6.15 | 2.32 |
| | G4 | 27.86 | 3.67 | 82.68 | 32.47 | 1.45 | 22.39 | 7.59 | 1.90 |

## 3.1. Load-Deflection Relationships

For evaluating the performance of the different reinforcement materials and concrete, first crack load, ultimate load, and corresponding deflection were recorded. The recorded ultimate loads and deflections for both the first and second groups, i.e., all four types of concrete mixture (normal concrete, HSC, GFRC, and HSC+glass fiber bristles), were higher than the reference specimen. The control specimen (C) recorded a first crack load and an ultimate load of 16.99 kN and 57.02 kN, respectively. In the first group, B1, B2, B3, and B4 showed a first crack of 18.78 kN, 24.88 kN, 21.71 kN, and 28.85 kN, respectively, and achieved an ultimate load of 57.02 kN, 76.15 kN, 80.02 kN, and 84.79 kN, respectively. For the second group, G1, G2, G3, and G4 showed a first crack of 16.04 kN, 25.51 kN, 19.37 kN, and 27.86 kN, respectively, and achieved an ultimate load of 72.85 kN, 78.13 kN, 73.87 kN, and 82.68 kN, respectively. The percentage improvement in ultimate capacity above C for the first group was 134%, 140%, 141%, and 149%, respectively. For the second group, the recorded ultimate capacity improvement was 128%, 137%, 130%, and 145%, respectively.

The control specimen recorded a deflection of 20.87 mm at the ultimate load. Deflection increased throughout all groups; the first group exhibited deflections of 31.63 mm, 33.20 mm, 30.73 mm, and 34.87 mm for the B1, B2, B3, and B4 specimens, respectively, at ultimate load. The second group showed deflection of 34.41 mm, 28.61 mm, 26.64 mm, and 32.47 mm for the G1, G2, G3, and G4 specimens, respectively.

## 3.2. Effect of Material Type

Higher values of ultimate load and deflection were seen in all footings reinforced with BFRP bars or GFRP bars when compared to the reference specimen at the same concrete mixtures (Figure 7). For the normal concrete mixture, the results showed an increase in ultimate load compared to the reference specimens for B1 and G1 by 34% and 28%, respectively. The HSC mixture demonstrated an ultimate load increase of 40% and 37%, respectively, when compared to the reference specimens for B2 and G2. The FRPC mixture demonstrated an ultimate load increase of 41% and 30%, respectively, when compared to the reference specimens for B3 and G3. The HSC+glass fiber bristles mixture demonstrated a 49% and 45% increase in ultimate load, respectively, compared to the reference specimens for B4 and G4. Generally, the CFRP performed better than GFRP in most cases as a result of the higher tensile strength and modulus of elasticity for BFRP compared with GFRP.

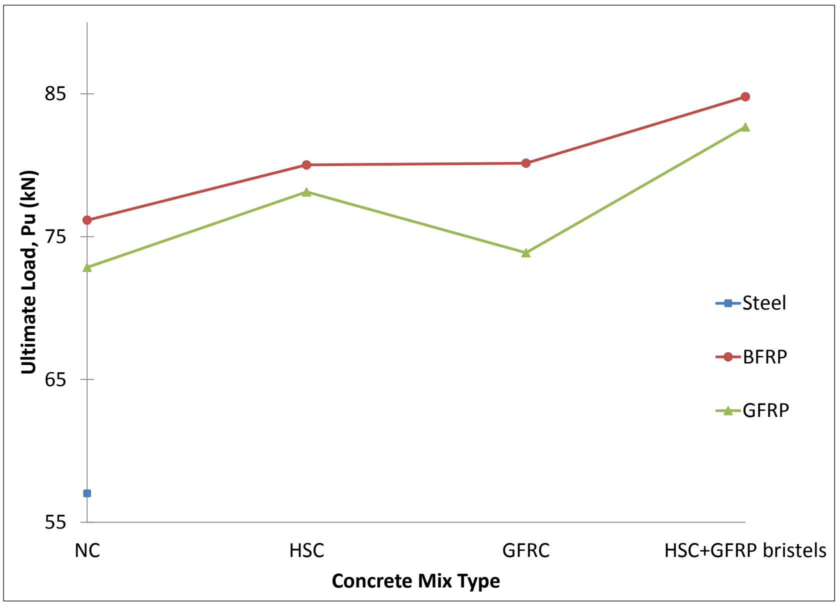


**Figure 7. Load capacity – type of material: a) rebar types b) concrete mixture type**

## 3.3. Stiffness

The ultimate stiffness (Ku) and uncracked stiffness (Ki) for all examined specimens were calculated using deflection and load measurements at the ultimate and cracking states, respectively (Table 5). The results indicate a notable increase in Ki for the first and second group specimens relative to the control sample, with increases of 1.82-2.08% and 1.76-2.32%, respectively. The reinforcement materials influenced the ultimate stiffness value (Ku), showing an increase for the specimens in the first and second groups by 6.97–8.19% and 6.15–7.59%, respectively.

## 3.4. Crack Propagation and Failure Characteristics

Figure 8 presents the crack patterns of failure at the footing face for all tested specimens. All specimens exhibited flexural failure as the mode of failure. With the increase in applied stress, the control specimen exhibited flexural cracks starting at the steel plate and extending towards the footing edge, particularly at the corners. The first crack appeared at loads in the range of 16 kN to 28 kN; the crack then continued to widen and gradually propagate to the edges until reaching a failure at loads ranging between 57 kN to 84 kN. The experimental observation showed that specimens reinforced with BFRP bars can withstand slightly greater loads before the beginning of the first crack and the failure load.

Figure 8-a shows the crack development in specimens reinforced with BFRP bars, while Figure 8-b shows the crack development in specimens reinforced with GFRP bars. The crack formation was noted in a multidirectional pattern. The GFRP and BFRP bars influenced the load distribution throughout the concrete surface, where the load was divided into lesser magnitudes for both directions.

The experiments also show that the addition of glass fiber to concrete has a significant effect on the crack pattern of reinforced concrete footing. The experimental observation indicated that the addition of glass fibers enhances the tensile strength of concrete, thereby decreasing cracking. The research indicated that the fibers serve as reinforcement, inhibiting crack growth and enhancing the concrete's endurance. Furthermore, the study found that the presence of glass fibers promotes a more uniform crack distribution in the concrete, enhancing the material's appearance. Glass fibers improve the tensile strength and ductility of concrete, which can enhance load-bearing capacity by delaying crack propagation and improving post-cracking behavior. Glass fibers reduce the permeability of concrete to chloride-ions due to crack prevention. The improved tensile strength and reduced shrinkage cracking from glass fibers can enhance the interface between concrete and FRP bars. Overall, the results of this research study suggest that incorporating glass fibers into concrete can result in a stronger, more durable material with a more desirable crack pattern. This is an improvement in the crack pattern, and the failure mode was found to be directly correlated with adding the fiber to the concrete mixture [5].

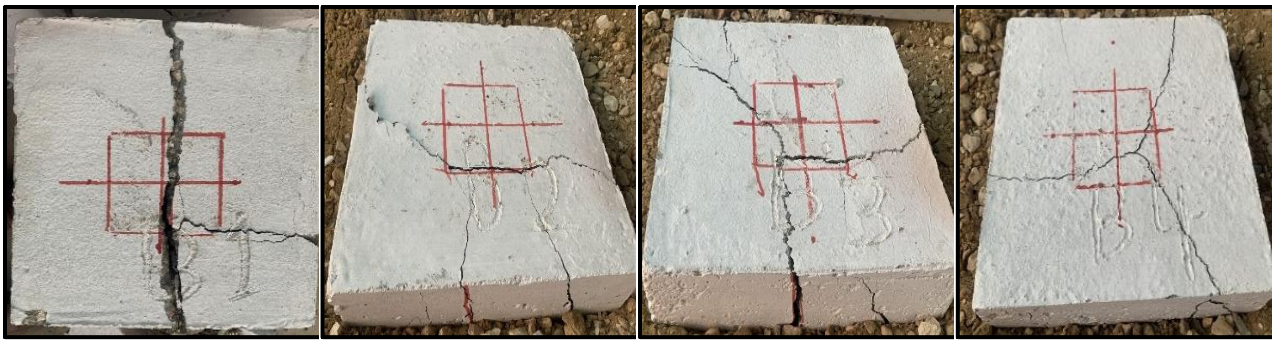

**B1** **B2** **B3** **B4**

(a) Specimens reinforced with BFRP bars

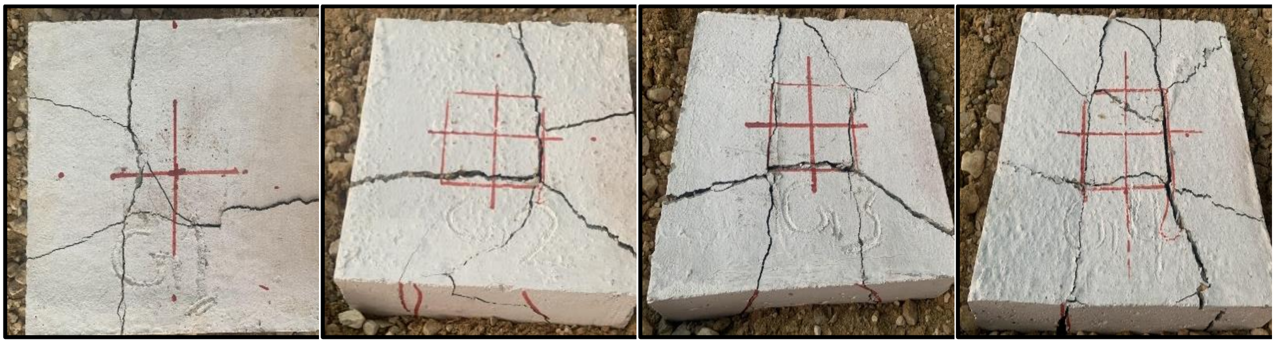

**G1** **G2** **G3** **G4**

(b) Specimens reinforced with GFRP bars

**Figure 8. Crack patterns at failure load of the tested footings**

# 4. Non-Linear Finite Element Analysis

## 4.1. General

To model the performance of an RC square footing reinforced with innovative materials, a nonlinear finite element analysis (FEA) was conducted using the Abaqus/CAE standard 2.7.3 software [34]. The modelling process took into account several factors including various types of elements and material characteristics, part assembly and interactions, loading conditions, steps interaction, and support types [35]. The subsequent sections present a summary of the elements used in this study to model the soil, concrete types (normal concrete, HSC, GFRC, and HSC with glass fiber bristles), reinforcing bars (steel, BFRP, and GFRP), steel support, and boundary conditions.

## 4.2. Materials Properties

To accurately replicate the experimental setup, the same material properties used in the experimental program for the soil, concrete (normal, HSC, GFRC, and HSC with glass fiber bristles), and reinforcement bars (steel, BFRP, and GFRP) were input into the Abaqus program. These properties included friction, cohesion, modulus of elasticity, and density of the soil and concrete, the concrete compressive strength, as well as the yielding stress, tensile strength and the elastic modulus of the steel, the GFRP and the BFRP bars.

## 4.3. Modelling Descriptions and Concrete-Reinforcement Boundary

A 3D deformable solid part was included in the model to represent the soil, RC square footing, and end supports, while 3D deformable wire elements were used for the steel, BFRP, and GFRP reinforcement bars. Choosing the right mesh density is a key factor in FEA. In this study, the mesh size was set to 100 mm for the soil and 10 mm for the RC footing in all directions. Mesh sensitivity analyses showed that a further decrease of the mesh size resulted in no major. enhancements. result accuracy. The reinforcement was modelled as an embedded element within the concrete 3D solid part. Three materials—steel, GFRP, and BFRP—were used to simulate the reinforcement bars, with a linear stress-strain curve defined for each. The model included the full-scale RC footing, and as shown in Figure 9, the parts assembly was designed to incorporate the RC square footing geometry at the load application point.

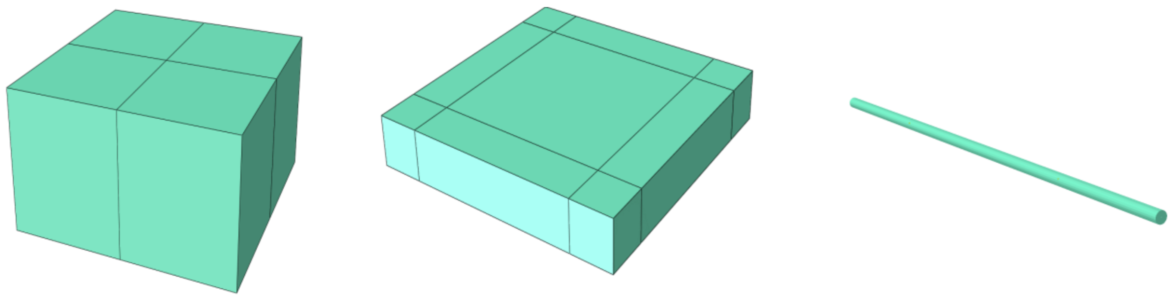

(a) Soil Part (b) Concrete footing part (c) Rebar

(d) Assembly (e) Boundary condition of soil bottom surface

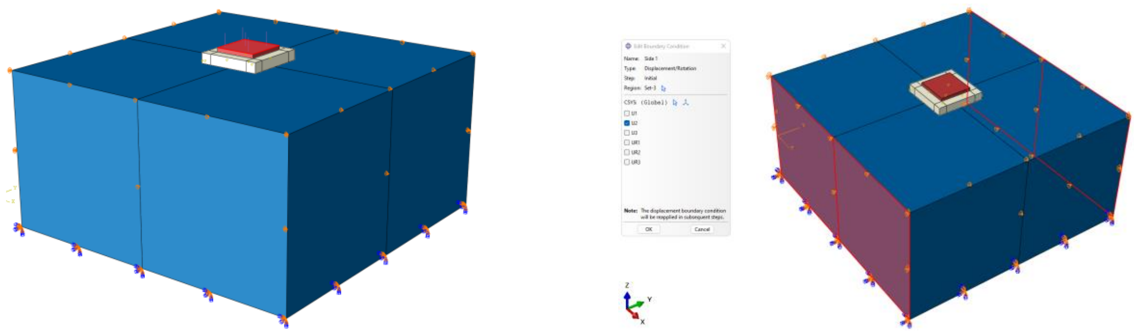

(f) Loading (g) Boundary condition of soil side surface

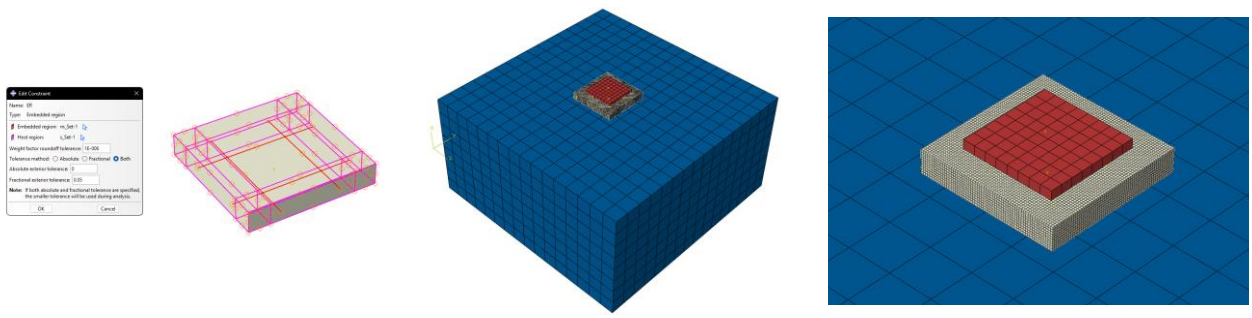

(h) Interaction and meshing of model

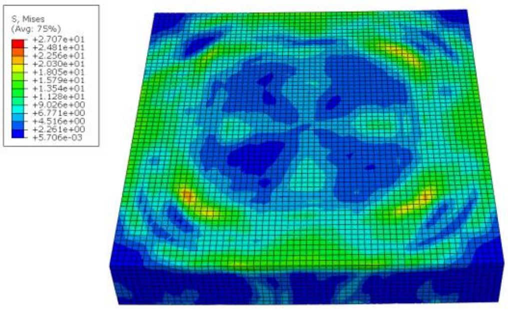

(i) Stresses

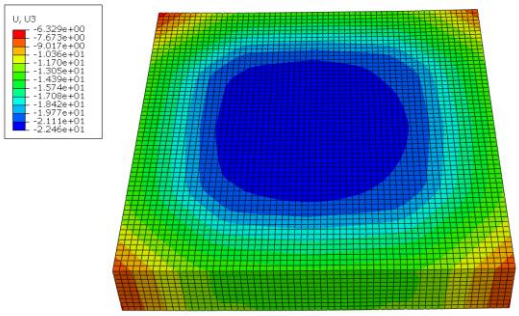

(j) Displacement

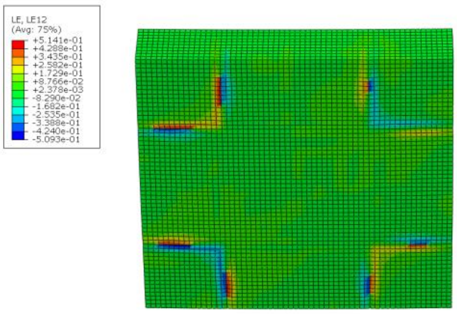

(k) Concrete strain

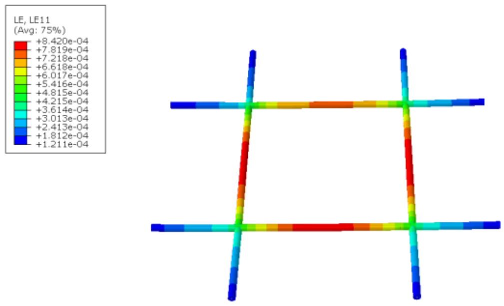

(l) Rebar stress

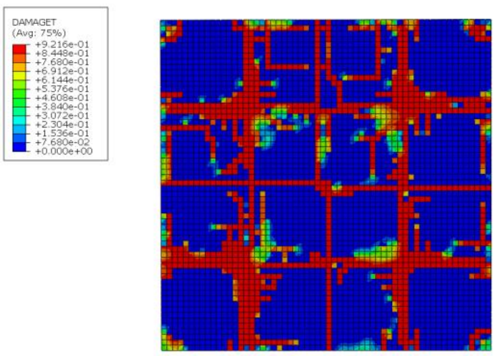

(m) FEM reference cracks

(n) Experimental reference crack

**Figure 9. Finite Element simulation of RC square footings**

### 4.4. Solution Control

The nonlinear finite element model developed in the ABAQUS program can involve thousands of variables, so to capture the non-linear effects, the total load is divided into multiple load steps. A 1-ton load is applied at each step. By default, ABAQUS updates the solution at the end of each step and utilizes it for the subsequent step, thus accounting for non-linearity. The solution is defined by a series of small increments, with each increment being solved before determining the size of the next one. The nonlinear equilibrium equations are solved numerically using Newton's method as the solver. This Newton's method was favored for having a superior convergence rate relative to alternative methods when solving the nonlinear problems that ABAQUS is commonly used to address.

### 4.5. Experimental, FEM and Theoretical Results

The FEM simulation results were confirmed by comparing them with the experimental data from control footing specimens. Once the FEM model was verified, it was applied to the other reinforcement experimental results to further validate its performance. Figure 10 shows the load-deflection curves for both the experimental and FEM results. The comparison confirmed that the FEM model is accurately represented in the load-deflection relationship observed in the experiments. Additionally, Figure 11 displays the crack patterns of the FEM specimens. Table 6 summarizes the comparison between the experimental and FEM results, while Figure 12 highlights the strong agreement between the experimental and FEM data for ultimate loads.

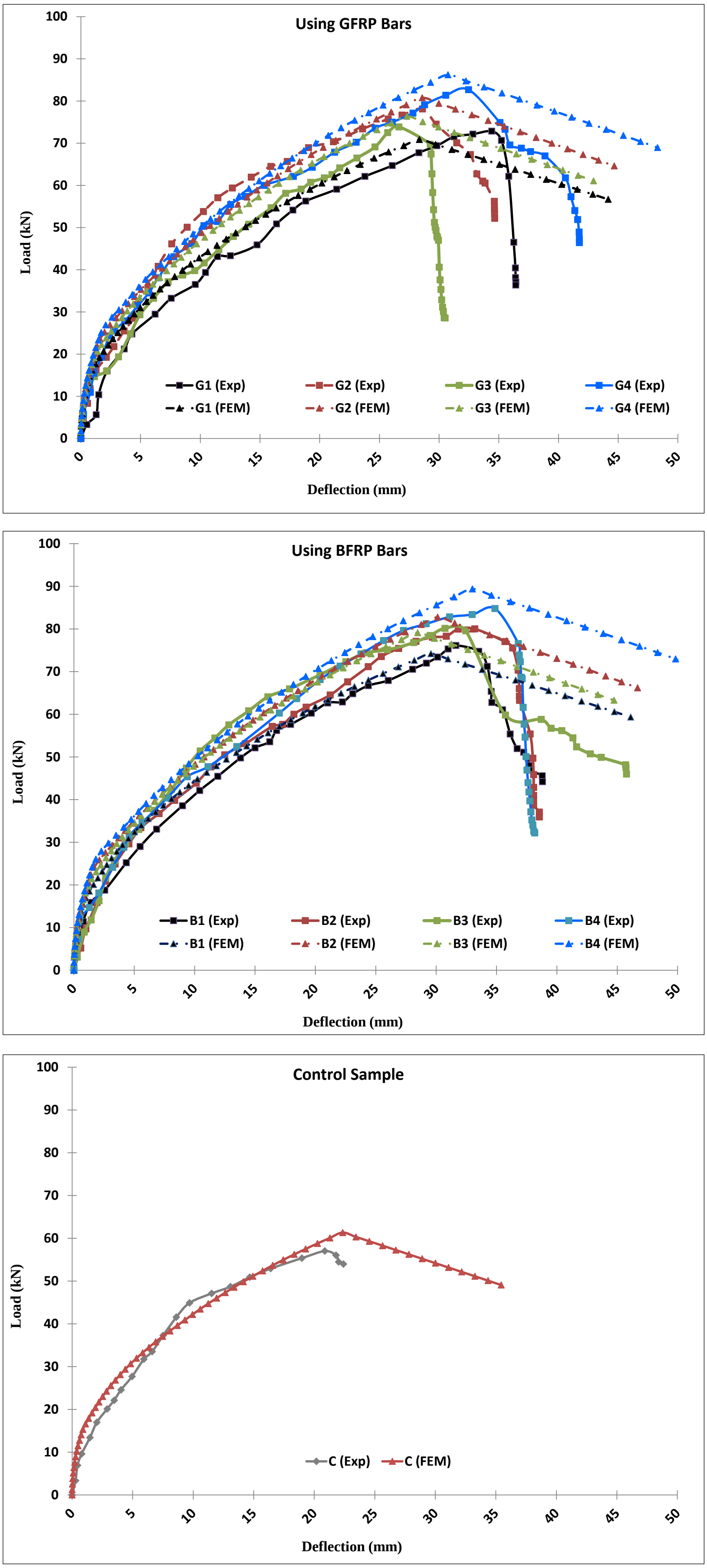


**Figure 10. Load-Deflection comparison between FEM and experimental result**

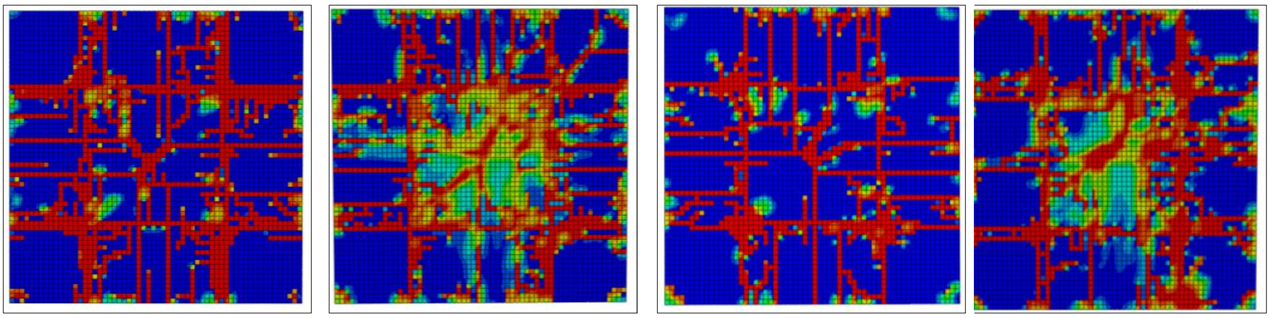

B1 B2 B3 B4

(a) Specimens reinforced with BFRP bars

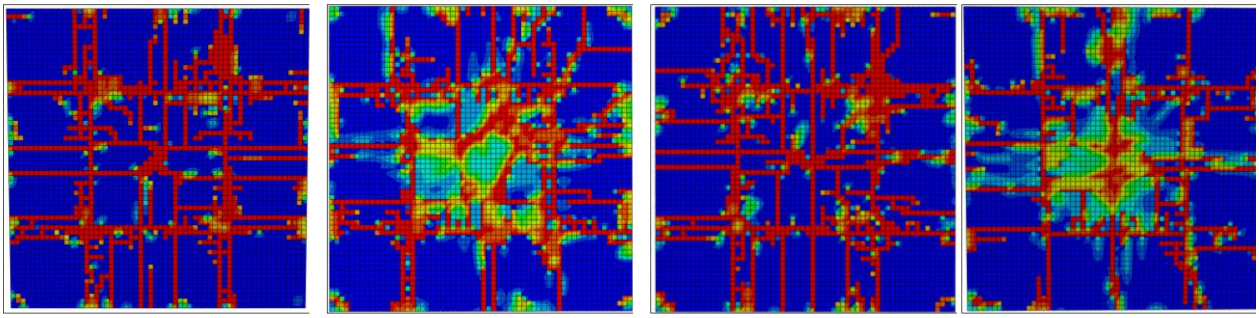

G1 G2 G3 G4

(b) Specimens reinforced with GFRP bars

**Figure 11. FEM results showing the crack patterns for all specimens**

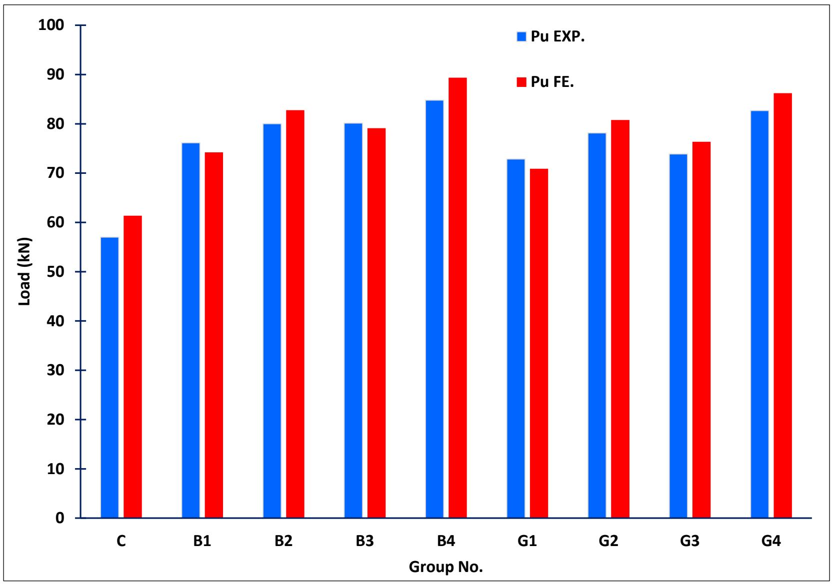


**Figure 12. Comparison between experimental and ultimate FEM loads**

**Table 6. Experimental, and finite element results comparison**

| Group No. | Reinforcement Material | Pu $_{EXP.}$ (kN) | P$_{FE.}$ (kN) | Pu $_{FE}$/ Pu $_{EXP}$ |
|---|---|---|---|---|
| C | Steel | 57.02 | 61.36 | 1.08 |
| B1 | BFRP | 76.15 | 74.21 | 0.97 |
| B2 | | 80.02 | 82.76 | 1.03 |
| B3 | | 80.14 | 79.12 | 0.99 |
| B4 | | 84.79 | 89.37 | 1.05 |
| G1 | GFRP | 72.85 | 70.88 | 0.97 |
| G2 | | 78.13 | 80.77 | 1.03 |
| G3 | | 73.87 | 76.37 | 1.03 |
| G4 | | 82.68 | 86.21 | 1.04 |
| | | | Mean | 1.02 |
| | | | SD | 0.04 |

# 5. Conclusions

This work included a series of experimental tests to investigate the ultimate load capacity of RC square footings reinforced with various commercially available materials. The reinforcement materials ranged from glass fiber bars to basalt fiber bars that were embedded in different types of concrete mixtures, namely normal concrete, high-strength concrete, glass fiber reinforced concrete, and high-strength concrete with glass fiber bristles. The experimental data were used to prove the nonlinear methodology employed in the FEA and to predict the performance of the different materials. The following conclusions are also brought forward:

- Employing various concrete mixtures enhanced the ultimate load of the reinforced concrete footing compared to the control. The ultimate load increased between 34% to 49% for specimens reinforced with BFRP bars, while it increased between 28% to 45% for specimens reinforced with GFRP bars.
- Using FRP bars enhances the ultimate load of the RC footing at the same concrete mixture compared to the control. For normal concrete, the ultimate load increased by 34% and 28% for specimens reinforced with BFRP and GFRP bars, respectively. For the high-strength concrete mixture, the ultimate load increased by 40% and 37% for B2 and G2, respectively. For the HSC mixture, the ultimate load increased by 40% and 37% for B2 and G2, respectively. For the GFRC mixture, the ultimate load increased by 41% and 30% for B3 and G3, respectively. For the HSC+GFRP bristles mixture, the ultimate load increased by 49% and 45% for B4 and G4, respectively.
- Applying BFRP bars enhanced the ultimate load capacity when compared to GFRP bars using the same concrete mixture.
- The usage of FRP bars increased deflection in all specimens relative to the control sample.
- The utilization of FRP bars with various concrete mixtures resulted in a reduction of ultimate stiffness by 6.15–8.19% when compared to the control.
- All specimens exhibit flexural failure as the mode of failure. FRP bars influence the load distribution across the concrete surface, hence enhancing cracking. The addition of glass fibers improves the tensile strength of concrete, thereby reducing cracking.
- Nonlinear finite element analysis has been validated and proved significant convergence with the experimental results.

# 6. Declarations

## 6.1. Author Contributions

Conceptualization, M.A. and M.I.B.; methodology, M.A. and M.I.B.; software, M.I.B.; data curation, M.I.B.; writing—original draft preparation, M.I.B.; writing—review and editing, M.A.; visualization, M.I.B. and M.A.; supervision, M.A. All authors have read and agreed to the published version of the manuscript.

## 6.2. Data Availability Statement

The data presented in this study are available in the article.

## 6.3. Funding

The authors received no financial support for the research, authorship, and/or publication of this article.

## 6.4. Conflicts of Interest

The authors declare no conflict of interest.

# 7. References

[1] El-Sayed, T. A., Abdallah, K. S., Ahmed, H. E., & El-Afandy, T. H. (2023). Structural Behavior of Ultra-High Strength Concrete Columns Reinforced with Basalt Bars Under Axial Loading. International Journal of Concrete Structures and Materials, 17(1), 1103. doi:10.1186/s40069-023-00600-9.

[2] Badawi, M. I., Awwad, M., Roshdy, M., & El-Kasaby, E. S. A. (2024). Investigation of an Innovative Technique for R.C. Piles Reinforced by Geo-Synthetics Under Axial Load. Civil Engineering Journal (Iran), 10(10), 3292–3306. doi:10.28991/CEJ-2024-010-10-011.

[3] Makhlouf, M. H., Ismail, G., Abdel Kreem, A. H., & Badawi, M. I. (2023). Investigation of transverse reinforcement for R.C flat slabs against punching shear and comparison with innovative strengthening technique using FRP ropes. Case Studies in Construction Materials, 18(2), 1935. doi:10.1016/j.cscm.2023.e01935.

[4] El-kasaby, E. S. A., Awwad, M., & M. Mansour, A. (2023). Experimental study of glass fiber concrete piles reinforced with GFRP bars and geogrid under concentric loads. International Journal of Advanced Engineering, Management and Science, 9(9), 66–74. doi:10.22161/ijaems.99.7.

[5] El-Kasaby, E.-S. A., Awwad, M., Roshdy, M., & Abo-Shark, A. A. (2023). Behavior of Square Footings Reinforced with Glass Fiber Bristles and Biaxial Geogrid. European Journal of Engineering and Technology Research, 8(4), 5–11. doi:10.24018/ejeng.2023.8.4.3075.

[6] Hadad, H. S., Nooman, M. T., & Saleh, K. A. (2021). Behaviors of isolated footings reinforced with glass fiber bars. Al-Azhar University Civil Engineering Research Magazine, 43(2), 35–48.

[7] Latha, G. M., & Somwanshi, A. (2009). Bearing capacity of square footings on geosynthetic reinforced sand. Geotextiles and Geomembranes, 27(4), 281–294. doi:10.1016/j.geotexmem.2009.02.001.

[8] El-Nemr, A., Ahmed, E. A., & Benmokrane, B. (2013). Flexural Behavior and Serviceability of Normal-and High-Strength Concrete Beams Reinforced with Glass Fiber-Reinforced Polymer Bars. ACI structural journal, 110(6). doi:10.14359/51686162.

[9] Maranan, G. B., Manalo, A. C., Benmokrane, B., Karunasena, W., & Mendis, P. (2015). Evaluation of the flexural strength and serviceability of geopolymer concrete beams reinforced with glass-fibre-reinforced polymer (GFRP) bars. Engineering Structures, 101, 529–541. doi:10.1016/j.engstruct.2015.08.003.

[10] Elgabbas, F., Vincent, P., Ahmed, E. A., & Benmokrane, B. (2016). Experimental testing of basalt-fiber-reinforced polymer bars in concrete beams. Composites Part B: Engineering, 91, 205–218. doi:10.1016/j.compositesb.2016.01.045.

[11] Li, Z., Zhu, H., Du, C., Gao, D., Yuan, J., & Wen, C. (2021). Experimental study on cracking behavior of steel fiber-reinforced concrete beams with BFRP bars under repeated loading. Composite Structures, 267, 113878. doi:10.1016/j.compstruct.2021.113878.

[12] Mohamed, O. A., Hawat, W. Al, & Keshawarz, M. (2021). Durability and mechanical properties of concrete reinforced with basalt fiber-reinforced polymer (BFRP) bars: Towards sustainable infrastructure. Polymers, 13(9), 1402. doi:10.3390/polym13091402.

[13] Wu, Z., Wang, X., & Wu, G. (2012). Advancement of structural safety and sustainability with basalt fiber reinforced polymers. Proceedings of the 6th International Conference on FRP Composites in Civil Engineering, CICE 2012, 13-15 June, 2012, Rome, Italy.

[14] Patnaik, A., Puli, R., Mylavarapu, R., & Basalt, F. R. P. (2004). A new FRP material for infrastructure market. Proceedings 4th International Conference Advanced Composite Materials in Bridges and Structures (ACMBS-IV), 20-23 July, 2024, Calgary, Canada.

[15] Serbescu, A., Guadagnini, M., & Pilakoutas, K. (2015). Mechanical Characterization of Basalt FRP Rebars and Long-Term Strength Predictive Model. Journal of Composites for Construction, 19(2), 143. doi:10.1061/(asce)cc.1943-5614.0000497.

[16] Vincent, P., Ahmed, E., & Benmokrane, B. (2013). Characterization of basalt fiber-reinforced polymer (BFRP) reinforcing bars for concrete structures. Proceedings of the 3rd Specialty Conference on Material Engineering & Applied Mechanics, 29 May-1 June, Montreal, Canada.

[17] Elgabbas, F., Ahmed, E. A., & Benmokrane, B. (2015). Physical and mechanical characteristics of new basalt-FRP bars for reinforcing concrete structures. Construction and Building Materials, 95, 623–635. doi:10.1016/j.conbuildmat.2015.07.036.

[18] Tomlinson, D., & Fam, A. (2015). Performance of Concrete Beams Reinforced with Basalt FRP for Flexure and Shear. Journal of Composites for Construction, 19(2), 712. doi:10.1061/(asce)cc.1943-5614.0000491.

[19] Banibayat, P., & Patnaik, A. (2015). Creep Rupture Performance of Basalt Fiber-Reinforced Polymer Bars. Journal of Aerospace Engineering, 28(3), 4014074. doi:10.1061/(asce)as.1943-5525.0000391.

[20] Patnaik, A. (2009). Applications of basalt fiber reinforced polymer (BFRP) reinforcement for transportation infrastructure. Developing a Research Agenda for Transportation Infrastructure -TRB, November 2009, 1-5.

[21] Brik, V. (2003). Advanced concept concrete using basalt fiber/BF composite rebar reinforcement. Final Report for Highway-IDEA Project 86, Transportation Research Broad, Washington, United States.

[22] Sim, J., Park, C., & Moon, D. Y. (2005). Characteristics of basalt fiber as a strengthening material for concrete structures. Composites Part B: Engineering, 36(6–7), 504–512. doi:10.1016/j.compositesb.2005.02.002.

[23] Benmokrane, B., Elgabbas, F., Ahmed, E. A., & Cousin, P. (2015). Characterization and Comparative Durability Study of Glass/Vinylester, Basalt/Vinylester, and Basalt/Epoxy FRP Bars. Journal of Composites for Construction, 19(6), 34. doi:10.1061/(asce)cc.1943-5614.0000564.

[24] Halim, N. H. F. A., Alih, S. C., Vafaei, M., Baniahmadi, M., & Fallah, A. (2017). Durability of fibre reinforced polymer under aggressive environment and severe loading: A review. International Journal of Applied Engineering Research, 12(22), 12519–12533.

[25] Wei, B., Cao, H., & Song, S. (2010). Environmental resistance and mechanical performance of basalt and glass fibers. Materials Science and Engineering: A, 527(18–19), 4708–4715. doi:10.1016/j.msea.2010.04.021.

[26] Gu, C. P., Ye, G., & Sun, W. (2015). Ultrahigh performance concrete-properties, applications and perspectives. Science China Technological Sciences, 58(4), 587–599. doi:10.1007/s11431-015-5769-4.

[27] Ahmed, E. A., Benmokrane, B., & Sansfaçon, M. (2017). Case Study: Design, Construction, and Performance of the La Chancelière Parking Garage's Concrete Flat Slabs Reinforced with GFRP Bars. Journal of Composites for Construction, 21(1), 68. doi:10.1061/(asce)cc.1943-5614.0000656.

[28] Sagar, B., & Sivakumar, M. V. N. (2021). Performance evaluation of basalt fibre-reinforced polymer rebars in structural concrete members–a review. Innovative Infrastructure Solutions, 6(2), 423. doi:10.1007/s41062-020-00452-2.

[29] Afroughsabet, V., Biolzi, L., & Ozbakkaloglu, T. (2016). High-performance fiber-reinforced concrete: a review. Journal of Materials Science, 51(14), 6517–6551. doi:10.1007/s10853-016-9917-4.

[30] Christian, A., & Chye, G. O. K. (2014). Performance of fiber reinforced high-strength concrete with steel sandwich composite system as blast mitigation panel. Procedia Engineering, 95(9), 150–157. doi:10.1016/j.proeng.2014.12.174.

[31] Ezzsteel. (2025). EZZ STEEL, Cairo, Egypt. Available online: https://www.ezzsteel.com/ (accessed on March 2025).

[32] Armastek (2025). Armastek and imported by Fiber Reinforcement Industries Company. Armastek, Johannesburg, South Africa. Available online: https://armastek-za.com/ (accessed on March 2025).

[33] ABFC. (2025). Arab Basalt Fiber Company, Fujairah, United Arab Emirates. Available online: https://arabbasaltfiber.com/ (accessed on March 2025).

[34] Dassault Systems. (2017). Abaqus/CAE User's Manual. Dassault Systems, Vélizy-Villacoublay, France.

[35] Ali, A. H., Gouda, A., Mohamed, H. M., Rabie, M. H., & Benmokrane, B. (2020). Nonlinear finite elements modeling and experiments of FRP-reinforced concrete piles under shear loads. Structures, 28, 106–119. doi:10.1016/j.istruc.2020.08.047.